Journal of Macromolecular Science, Part A
Publication details, including instructions for authors and subscription information:
http://www.informaworld.com/smpp/title~content=t713597274

Synthesis, Optical and Photovoltaic Properties of Porphyrin Dyes

M. W. Lee[a]; D. L. Lee[a]; W. N. Yen[b]; C. Y. Yeh[b]
[a] Department of Physics, National Chung Hsing University, Taichung, Taiwan [b] Department of Chemistry, National Chung Hsing University, Taichung, Taiwan

To cite this Article Lee, M. W. , Lee, D. L. , Yen, W. N. and Yeh, C. Y.(2009) 'Synthesis, Optical and Photovoltaic Properties of Porphyrin Dyes', Journal of Macromolecular Science, Part A, 46: 7, 730 — 737
To link to this Article: DOI: 10.1080/10601320902938558
URL: http://dx.doi.org/10.1080/10601320902938558

Journal of Macromolecular Science®, Part A: Pure and Applied Chemistry (2009) **46**, 730–737

ISSN: 1060-1325 print / 1520-5738 online
DOI: 10.1080/10601320902938558

Taylor & Francis
Taylor & Francis Group

Synthesis, Optical and Photovoltaic Properties of Porphyrin Dyes

M. W. LEE[1,*], D. L. LEE[1], W. N. YEN,[2] and C. Y. YEH[2]

[1]*Department of Physics, National Chung Hsing University, Taichung, Taiwan*
[2]*Department of Chemistry, National Chung Hsing University, Taichung, Taiwan*

Received and Accepted January 2009

The synthesis and optical absorption of a series of porphyrins, and the photoelectrochemical properties of TiO_2 solar cells sensititized with these porphyrins was investigated. The different types of porphyrins studied are designated by numbers: the reference compound **1 (**Zinc(II) 5,15-bis(4-carboxylphenyl)porphyrin), porphyrin substituted with one triarylamine unit **2**, and porphyrin substituted with two triarylamine units **3**. The UV-Vis absorption spectra reveal that the substitutions result in large redshifts in both the Soret band (∼60 nm) and the Q bands (∼125 nm), as well as enhancement of optical absorption. The enhancement is even more pronounced in the long-wavelength region of 575–725 nm, where the absorption of porphyrin **3** is eight times that of porphyrin **1**. The photoelectrochemical properties of the porphyrins were also studied by constructing porphyrin-sensitized TiO_2 solar cells. Under standard AM 1.5 sunlight, the porphyrin **1** cell yields a short-circuit current of ∼1.26 mA/cm^2, an open-circuit voltage of ∼0.564 V, and a fill factor of ∼61%. The incident photon-to-current conversion efficiency is ∼24% for porphyrin **1** and ∼5–7% for porphyrins **2** and **3** at the Soret peak.

Keywords: Dye-sensitized solar cells, porphyrin, photoelectrochemical processes, optical absorption

1 Introduction

Dye-sensitized solar cells (DSSCs) are a promising candidate for a new generation of photovoltaic devices (1, 2). They are low-cost and suitable for large-scale production (3–5). Central to such a DSSC device is a 10 μm-thick electrode layer made of a nanoparticulate oxide (typically TiO_2) 20–30 nm in diameter. The particulate structure increases the surface area for dye chemisorptions to a thousand times that of a flat electrode of the same size (6). When coated with a layer of high light-absorbing dye, such as one of the ruthenium polypyridyl complexes (N3), DSSCs can achieve an energy conversion efficiency of 10.4% under AM 1.5 simulated sunlight (7). There are two factors that limit even higher conversion efficiencies in DSSCs: one is the limited diffusion length of photogenerated electrons, typically several microns; the other is the improper overlap between the dye-absorption spectrum and the solar spectrum. With an N3 dye an incident-photon-to-current conversion efficiency of 85% can be achieved (7, 8), but its main absorption region is concentrated in the short-wavelength region of the visible spectrum, i.e., 400–700 nm. However, the solar spectrum covers ultraviolet, visible and near-infrared (NIR). Indeed, over 60% of the total solar photon flux is at wavelengths $\lambda > 600$ nm with approximately 50% in the red and NIR spectrum at $600 < \lambda < 1000$ nm. This means that the N3 dye utilizes only one half of the solar photon flux. Hence, much effort has been devoted to develop new dyes with broader absorption ranges, especially in the red and NIR regions.

Porphyrin molecules, the building blocks for chlorophyll, play a vital role in the natural photosynthetic process. Porphyrins absorb strongly in the 400–450 nm range (Soret or B band) and weakly in the 500–700 nm region (Q band). The photosynthetic components in thylakoid membranes of the chloroplast are stacked into large antenna arrays which enhances their light-harvesting efficiency (9). There has been intensive research into artificial photonic assemblies based on porphyrins designed to mimic this natural photosynthetic process (10–12). One subject that has attracted a great deal of attention is the employment of porphyrins as a sensitizing dye for the TiO_2 electrode in DSSCs. For example, there is the extensive investigation of a representative system, zinc tetrakis (4-carboxyphenyl) porphyrin (ZnTCPP) and its free-base H2TCPP (13–17). Much work has been focused on modifying the molecular structure of porphyrin, including various metallation and substitution groups, as well as anchoring groups, and studying how this affects the photoelectrochemical properties of DSSCs (18, 19). The power conversion efficiencies

*Address correspondence to: M. W. Lee, Department of Physics, National Chung Hsing University, Taichung, Taiwan. E-mail: mwl@phys.nchu.edu.tw

reported for porphyrin DSSCs to date are typically in the range of 0.5–3% and have recently been enhanced to 5–7% (16–18, 20–25). Large inconsistencies exist among different groups, indicating that many factors that influence the performance of porphyrin DSSCs are not well understood.

Tsuda and Osuda have recently reported that the absorption bands of π-conjugated fused porphyrin arrays could be red-shifted into the infrared region (26). In this work, we report on the synthesis of three porphyrin derivatives, achieved by substituting different numbers of triarylamine units at the meso position. The effects of substitution were investigated by measuring the UV-Vis absorption, Fourier-transform, infrared spectra and emission spectra of the porphyrins. Significant redshifts in absorption bands were observed in substituted porphyrins. The photoelectrochemial properties of DSSCs sensitized with the porphyrins were studied, and the results for the three samples compared. Finally, we discuss possible factors that might affect the performance of the porphyrin solar cells.

2 Experimental

2.1 Synthesis of the Porphyrin Dyes

The sequence of reactions for porphyrin synthesis is depicted in Scheme 1. Porphyrin **4** was prepared from acid-catalyzed cyclization of dipyrrolemethane and appropriate benzaldehyde as shown in Scheme 1 (27). Subsequent iodination and metallation gave mono- and diiodoporphyrins (28). The porphyrinyl iodides **6** and **7** were coupled with ethynyltriarylamine by Sonogashira cross-coupling reaction to give the conjugated porphyrin-triarylamine hybrids **8** and **9** (29–32). Porphyrin esters **8** and **9** were saponified by NaOH, followed by acidification to generate their corresponding carboxylic acids **2** and **3**. The molecular structures of porphyrins **1**–**3** are shown in Figure 1. The characteristics of the porphyrins are listed in the following.

Porphyrin **1** (Zinc(II) 5,15-bis(4-carboxylphenyl) porphyrin): ^{1}H-NMR (400 MHz, DMSO-d$_6$) δ_H = 9.59 (d, J = 4.8 Hz, 4H), 8.72 (d, J = 4.4 Hz, 4H), 8.29 (d,

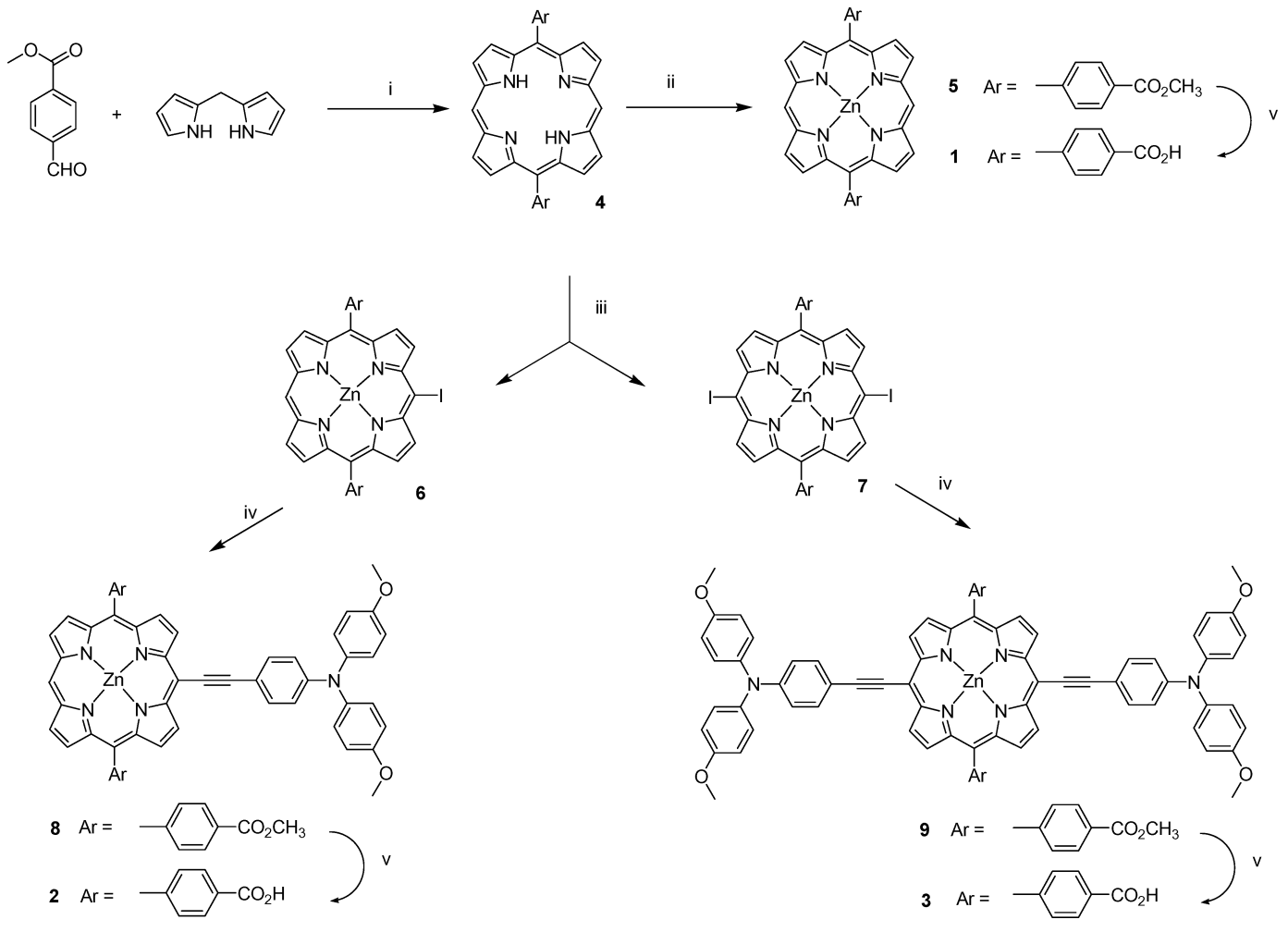

Sch 1. (i) (1) TFA, CH_2Cl_2, (2) DDQ, (ii) $Zn(OAc)_2.4H_2O$, CH_2Cl_2, CH_3OH, (iii) (1) $PhI(CF_3CO_2)_2$, I_2, $CHCl_3$, (2) $Zn(OAc)_2.4H_2O$, CH_2Cl_2, CH_3OH, (iv) N,N-Bis(4-methoxylphenyl)-N-(4-ethynylphenyl)amine, $Pd(PPh_3)_2Cl_2$, CuI, Et_3N, THF, (v) 20% NaOH(aq), CH_3OH, THF.

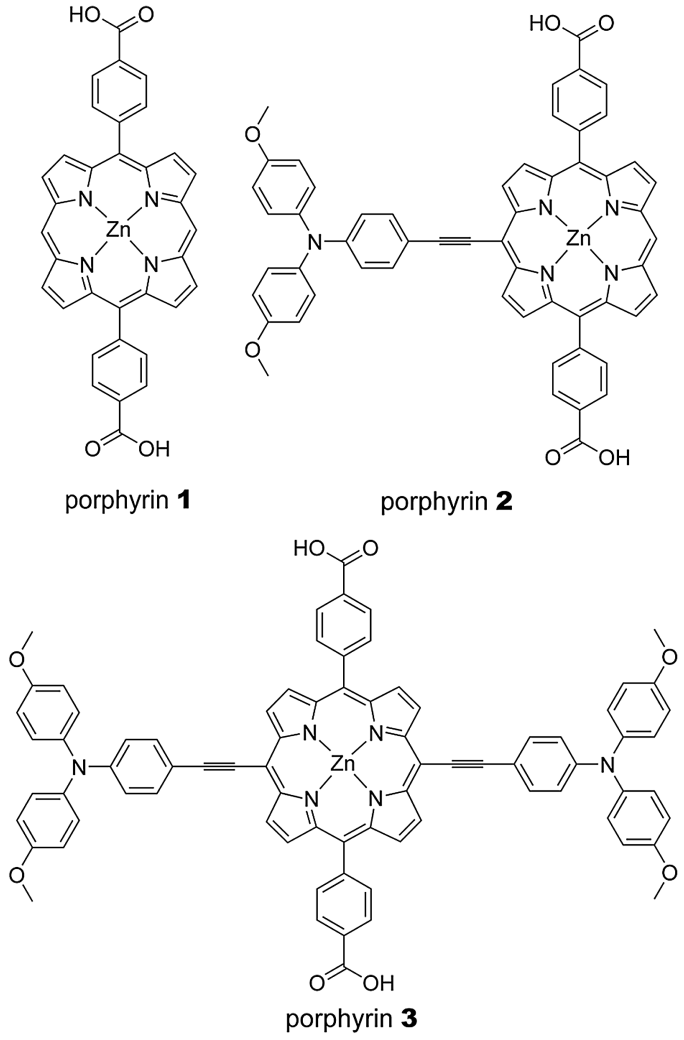

Fig 1. Molecular structures of porphyrins **1**–**3**.

J = 8.4 Hz,4H), 8.05 (d, J = 8.4 Hz, 4H), 7.87 (d, J = 8.8 Hz, 4H), 7.18 (d, J = 8.8 Hz, 8H), 7.00 (d, J = 8.8 Hz, 8H), 6.90 (d, J = 8.8 Hz, 4H), 3.78 (s, 12H); UV/Vis (CH_3OH) λ_{max}/nm (rel. ε) = 302(27), 466(100), 676(43); MS(FAB): 1266 m/z (M^+)

Porphyrin **2**: ^{1}H-NMR (400 MHz, DMSO-d_6) δ_H = 10.00 (s, 1H), 9.71 (d, J = 6.4 Hz, 2H), 9.24 (d, J = 6.0 Hz, 2H), 8.88 (t, J = 6.0 Hz, 4H), 8.38 (d, J = 10.40 Hz, 4H), 8.22 (d, J = 10.40 Hz, 4H), 7.76 (d, J = 11.40 Hz, 2H), 7.14 (d, J = 11.60 Hz, 4H), 6.99 (d, J = 11.60 Hz, 4H), 6.82 (d, J = 11.40, 2H), 3.72 (s, 6H) ; UV/Vis (CH_3OH) λ_{max}/nm (rel. ε) = 297(25), 455(100), 569(9), 624(21); MS(FAB): 941 m/z ($(M+H)^+$)

Porphyrin **3**: ^{1}H-NMR (400 MHz, DMSO-d_6) δ_H = 10.42 (s, 2H), 9.54 (d, J = 4.4 Hz, 4H), 8.94 (d, J = 4.4 Hz, 4H), 8.41 (d, J = 8.0 Hz, 4H), 8.35 (d, J = 8.0 Hz, 4H); UV/Vis (CH_3OH) λ_{max}/nm (rel. ε.) = 410(100), 544(4), 581(2).

2.2 Preparation of the TiO_2 Electrodes

The TiO_2 electrodes were prepared from a commercial colloidal TiO_2 paste: DSL 18NR-AO purchased from Dyesol Inc. The paste was spread onto a fluorine-doped SnO_2 conducting glass (FTO) (12 Ω/square, Asahi Glass Co.) and heated at 450°C (temperature rising rate 2°C/min) for 30 min. A thin layer of Nb_2O_5 was coated onto the electrode by treating it in a solution of 0.01 M of $NbCl_5$. This layer served the dual purpose of increasing electrical conduction and enhancing optical reflection. The thickness of the TiO_2film, determined by a surface profiler, was approximately 12 μm. The surface morphology of the finished TiO_2 electrode was examined using scanning electron microscopy (SEM) and atomic force microscopy (AFM).

2.3 Adsorption of the Porphyrin Dyes

The sintered TiO_2 electrode was sensitized by treating the electrode in a 0.3 mM methanol solution of the porphyrin dye at a temperature of T = 50–60°C for 24 h. The dye-sensitized electrode was left to dry at room temperature. An FTO glass with Pt foil 150 μm in thickness served as the counter electrode. The TiO_2 electrode and the counter electrode were assembled and sealed by utilizing a parafilm, 25 μm in thickness, as a spacer. The electrolyte solution was composed of 0.5 M of LiI, 0.05 M of I_2, 0.5 M of 4-tert-butylpyridine (TBP), and 0.6 M of 1-butylmethylimidazoilium iodide (BMII) in acetonitrile and valeronitrile. The active area of the cell was approximately 9 mm^2.

2.4 Spectroscopic and Analytical Methods

UV-Vis absorption spectra were measured with a Hitachi U-2800A spectrophotometer. The FTIR spectra were measured with a Jasco 410 spectrometer. The fluorescence spectra, recorded with a Varian Cary 100 Conc spectrometer, were measured by exciting the samples with a wavelength of 450 nm.

2.5 Photoelectrochemical Measurements

The spectral response was determined from the incident photon-to-current conversion efficiency (IPCE) measurements. For the IPCE measurements, the output of a 200 W tungsten halogen lamp was guided by an optical fiber into an Acton monochrometer, the dispersed light was then guided by an optical fiber onto the sample. The photogenerated current was measured using a Keithley 2400 sourcemeter. The wavelength-dependent IPCE can be calculated from the following equation:

$$\text{IPCE}\,(\%) = \frac{1240 \cdot J}{\lambda \cdot P} \times 100,$$

Where J is the current density (mA/cm^2), λ is the wavelength (nm), and P is the power of the incident light (mW/cm^2). During the IPCE measurements P was kept at a relatively low level, typically 6 μW. The reflectivity at the FTO surfaces resulted in a power loss of approximately 25%, which was taken into account in the IPCE calculation.

A 150 W xenon lamp (Oriel) was used as the light source for the current-voltage (I-V) measurements. The output of the lamp was focused by passing it through a filter that simulates the AM 1.5 (100 mW/cm^2) spectrum. It was then irradiated onto the sample. The I-V curves were measured by applying a biased voltage to the photocell, after which the photocurrent was recorded using a Keithley 2400 sourcemeter. The conversion efficiency η can then be calculated from the open-circuit voltage (V_{oc}), short-current density (J_{sc}), the fill factor (ff), and the intensity of the incident light (I_{ph})

$$\eta = \frac{J_{sc} \cdot V_{oc} \cdot ff}{I_{ph}}.$$

3 Results and Discussion

3.1 TiO_2 Electrode

SEM and AFM examination of the surface morphology of the produced TiO_2 film showed a three-dimensional network of interconnected particles having an average particle size of 30 nm. Figure 2 shows the AFM images of the TiO_2 film. The film was highly porous, which is required for the adsorption of the dye. Figure 3 shows the X-ray diffraction pattern of the TiO_2 film. The film consists mostly of the anatase phase and a small portion of the rutile phase. The particle size can be further estimated from the widths of the X-ray diffraction peaks using the Debye-Scherrer's equation:$d = k\lambda/\sqrt{A^2 - B^2\cos^2\theta}$, where d is the particle size, $k = 0.9$, λ is the wavelength of the X-ray (1.542 Å), θ is the diffraction angle, A is the width of the peak, and B is a background correction for the glass substrate (0.003 rad). Inserting the experimental data for a pronounced peak: $2\theta = 25.45^\circ$, $A = 0.006283$ rad, the average particle size d was 26 nm.

3.2 UV-Vis Absorption Spectra

The UV-Vis absorption spectra for the three types of porphyrin in tetrahydrofuran (THF) solution (molar concentration of 8×10^{-6} M) are shown in Figure 4. The spectra exhibit a series of visible bands due to the $\pi \rightarrow \pi^*$ transitions of the conjugated macrocycle. Porphyrin **1** (unsubstituted sample) has two bands in the violet region (the Soret band): 413 nm (the strongest), 389 nm (weak), and three weak bands in the green-yellow region (the Q bands): 506 (very weak), 543 and 581(weak) nm. The molar extinction coefficient ε of the largest peak of porphyrin **1** is $\sim 10^5 M^{-1}cm^{-1}$, which is consistent with other reports (22). In general, the absorption bands broadened and redshifted after substitution. The shifts in frequency for the Soret and Q bands are tabulated in Table 1. The large Soret band shifted from 413 to 451, then to 472 nm, a total change of 14%. The two Q band peaks also redshifted by a total of ~15%. The redshifts indicate a narrowing of the energy gap, $E_g = E_{LUMO} - E_{HOMO}$, where E_{LUMO} and E_{HOMO} are the energy of the lowest-unoccupied molecular orbital (LUMO) and the highest-occupied molecular orbital (HOMO), respectively. Theoretical calculation reveals that peripheral substitutions to porphyrin molecules lead to increases of energies in both the LUMO and the HOMO states (33). However, the increase in the former is significantly smaller than in the latter, resulting in a smaller energy gap. The amount of energy shift depends on the electronic properties and the location of the substituents on the porphyrin ring; it can also be affected by the distortion of the porphyrin ring from the planar structure.

The optical absorption of porphyrin**3** is markedly more enhanced in the visible spectral ranges of 425–725 nm than that of the unsubstituted porphyrin **1**, which has extremely weak absorption in the same range. For instance, the molar

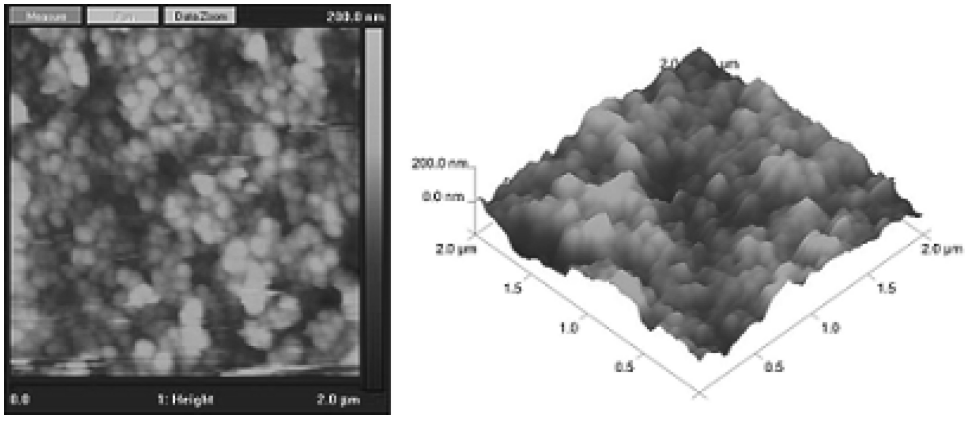

Fig 2. AFM images of the TiO_2 film.

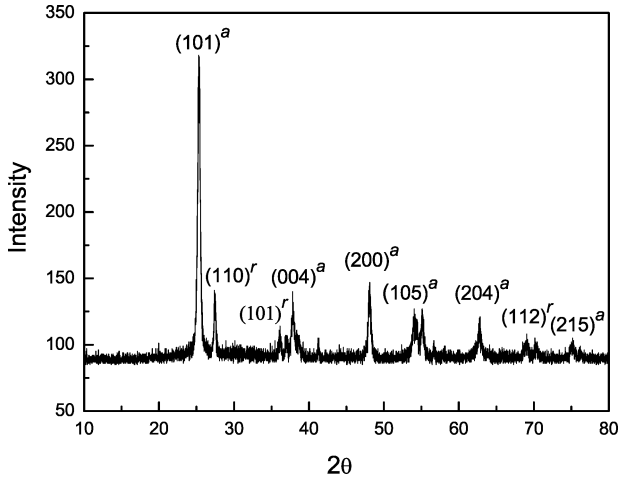

Fig 3. X-ray diffraction pattern of the TiO_2 film. The superscript *a* denotes the anatase phase and *r* denotes the rutile phase.

extinction coefficient ε at the $\lambda = 676$ nm peak is 25 times larger for porphyrin **3** than the corresponding ε for porphyrin **1**. The increase in absorption reflects the enhancement in oscillator strength for a given electronic transition. The area under the absorption curve represents the total optical absorption, or the number of carriers, n_e, participating in the optical absorption. This effect can be understood in terms of the optical sum rule (34)

$$\int \alpha d\omega = \frac{8\pi^2 e^2 n_e}{2mn},$$

where α is the optical absorption coefficient, e is the charge, m is the mass of carrier and n is the refractive index. Integrating the absorption curves over the whole spectral range of 375–725 nm yields the carrier ratio:

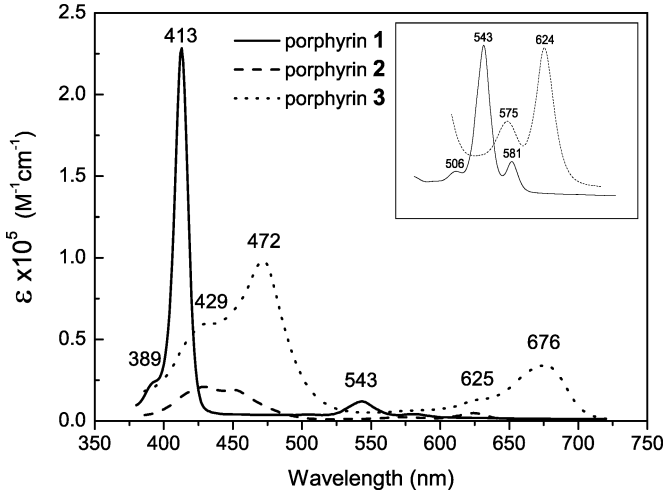

Fig 4. UV-Vis absorption spectra of porphyrins **1**–**3** in a THF solution. The inset shows enlarged B band peaks in the long-wavelength region for porphyrins **1** and **2**.

Table 1. Observed electronic absorption maxima for porphyrins **1**–**3**

Sample	λ (nm) *B Band*		λ *(nm) Q band*	
porphyrin **1**	389	413	543	581
porphyrin **2**	429	451	575	624
porphyrin **3**	429	472	625	676

$n_{e(\text{porphyrin}\mathbf{1})}$:$n_{e(\text{porphyrin}\mathbf{2})}$:$n_{e(\text{porphyrin}\mathbf{3})}$ = 1: 0.4: 2.1. The results indicate that porphyrin **3** is the best light absorber in the visible range whereas porphyrin **2** is the worst. Porphyrin **3** absorbs more than two times more visible light than porphyrin **1**. The effect is even more pronounced in the long-wavelength region of 575–725 nm, where the optical absorption of porphyrin **3** is eight times larger than that of porphyrin **1**.

3.3 FTIR Spectra

Fourier-transform infrared spectroscopy is a common technique for the investigation of the adsorption states of dye molecules on the surface of TiO_2 nanoparticles. Figure 5(a) shows the FTIR spectrum of porphyrin **1:** (A) in an ethanol solution, (B) adsorbed onto TiO_2, over the spectral range of 1000–2000 cm^{-1}. The solution spectrum, which

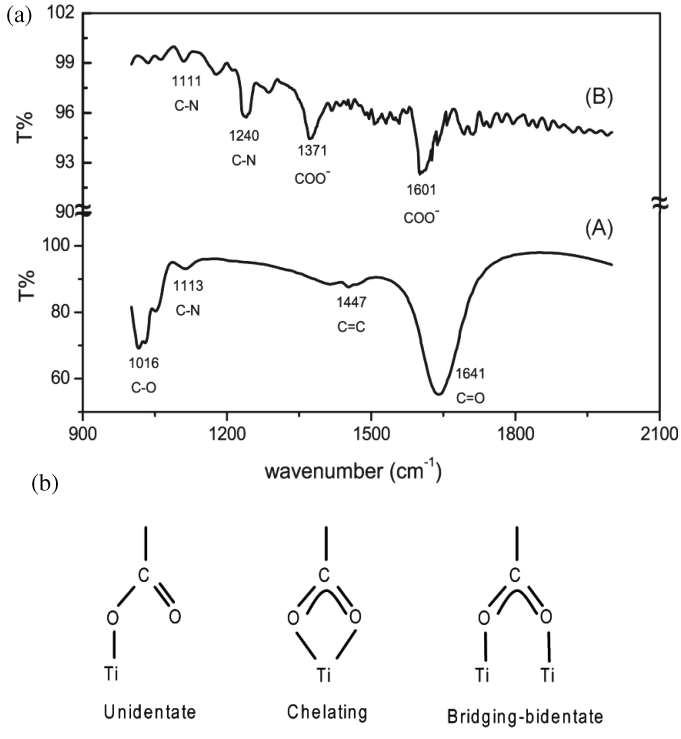

Fig 5. (a) FTIR spectra of porphyrin **1:** curve A: in an ethanol solution; curve B: adsorbed onto TiO_2, (b) Three possible carboxylate anchoring modes.

corresponds to the free-state of the molecule, shows a strong peak at 1641 cm^{-1}, which can be attributed to the ν(C=O) stretching mode of the carboxylic acid group. The two weak peaks at 1016 and 1113 cm^{-1} are attributable to the ν(C–O) and ν(C–N) modes of the macrocycle, respectively. When a porphyrin molecule was adsorbed onto TiO_2, the ν(C=O) mode (1641 cm^{-1}) disappeared and two new peaks appeared at 1601 and 1371 cm^{-1} are attributable to the asymmetric $\nu(-COO^-_{as})$ and symmetric $\nu(-COO^-_s)$ modes, respectively. There are three probable binding modes (illustrated in Figure 5 (b)): unidentate, chelating and bridging bidentate–binding a porphyrin molecule containing carboxylic acid groups onto a TiO_2 surface. On the basis of the FTIR spectra, the unidendate mode can be ruled out, because the stretching C=O mode is absent in the absorbed state. This leaves two possible modes: chelating and bridging bidentate. However, the chelating mode is known to be unstable (35). Consequently, the carboxylate group is most likely anchored to the TiO_2 surface via a bridging-bidentrate mode.

3.4 Emission Spectra

The emission spectra for the porphyrins are shown in Figure 6. Two emission peaks appeared at 638 and 700 nm in all three samples. The two peaks have also been observed in other porphyrins with various substitutions (36); they can be assigned as due to relaxation from the zero and hot vibronic levels of the lowest singlet excited state, S1. As can be seen in the figure, substitution led to a decrease in the intensity of the 638 nm peak and an increase in the intensity of the 700 nm peak, indicating changes in oscillator strength.

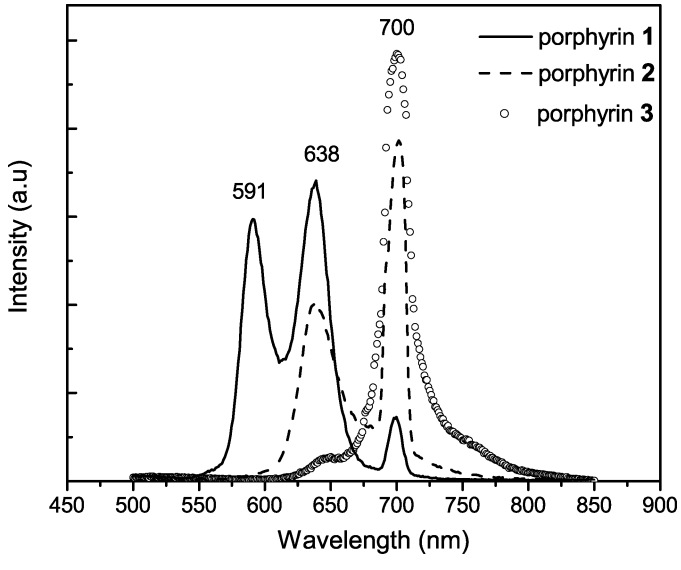

Fig 6. Emission spectra of porphyrins **1**–**3**.

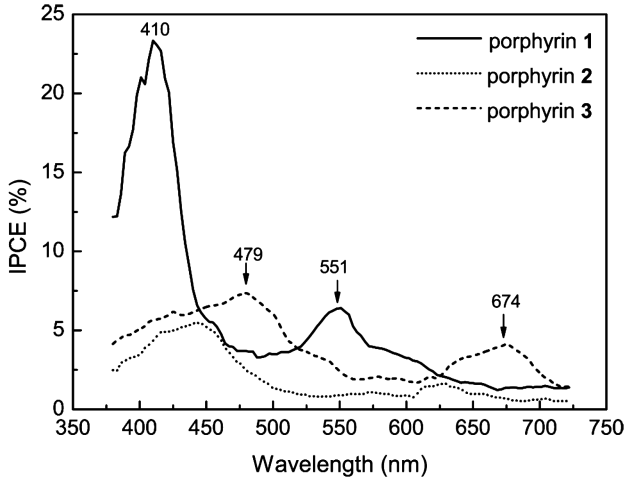

Fig 7. Photocurrent action spectra of porphyrins **1**–**3** anchored onto TiO_2 films.

3.5 Photocurrent Action Spectra and Current-Voltage Curves

The photocurrent action spectra for the porphyrin-sensitized solar cells are shown in Figure 7. The IPCE spectra are similar in shape, but broader than the absorption spectra in Figure 4. Porphyrin **1** (unsubstituted) has the largest conversion efficiency, 26% at $\lambda = 410$ nm. Porphyrin **3** has better IPCEs in the red-color region.

Figure 8 shows the current-voltage curves of the samples. The performance characteristics of the cells are listed in Table 2. Porphyrin **1** has the best performance, porphyrin **3** has the second best, and porphyrin **2** the poorest. The open-circuit voltages of the three samples range from 0.50 to 0.56 V and vary slightly with the samples. The main performance difference is with the current density.

The energy conversion efficiencies observed herein are low in comparison with other works. The problem is due

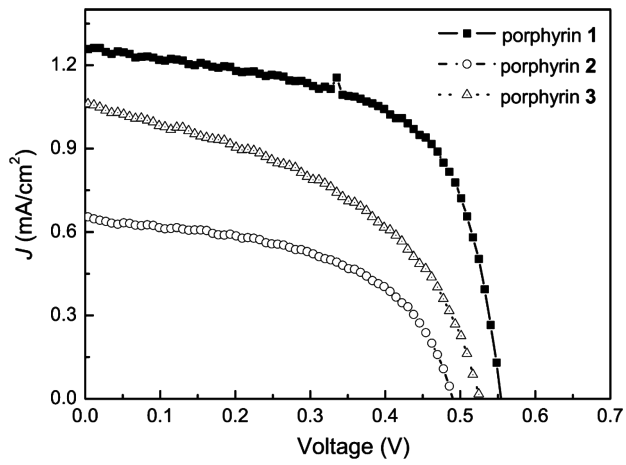

Fig 8. Photocurrent-voltage characteristics of the solar cells sensitized with porphyrins **1**–**3**.

Table 2. Photovoltaic performance of nanocrystalline TiO_2 films sensitized by porphyrin dyes. The active area is $0.3 \times 0.3\,cm^2$

Sample	V_{oc} *(V)*	J_{sc} J_{sc} *(mA/cm²)*	*ff (%)*	*η (%)*
porphyrin **1**	0.564	1.26	61.1	0.61
porphyrin **2**	0.501	0.75	52.3	0.26
porphyrin **3**	0.524	1.05	42.6	0.45

to the low IPCEs of the porphyrins. As Figure 7 indicates, the IPCEs of the substituted porphyrins were only ~5–7%. In contrast, the IPCEs of high-efficiency DSSCs normally reach 70–80%, more than an order of magnitude larger than our results. Low IPCEs mean that the photons absorbed by the porphyrin dye do not convert to photocurrent efficiently. We attribute this to two effects associated with the porphyrin dyes: (1) aggregation of the porphyrin molecules and (2) geometrical structure of the anchoring group. Organic dyes have been shown to aggregate strongly on the TiO_2 surface. Emission quenching measurements revealed that the aggregation reduces the injection yield of the photocarriers from the photoexcited dye into the conduction band of TiO_2 (37, 38). The reduction can reach an order of magnitude. In addition, the aggregation effect becomes stronger as the molecule size increases. This would explain the results that the substituted porphyrins, which are larger molecules, have lower IPCEs than the unsubstituted porphyrin. The second reason for low IPCEs is due to the geometrical structure of the anchoring group. Electron injection efficiency depends on the substituent and the position at which the substituent is anchored to the porphyrin molecule. In order to produce large conversion efficiencies, the porphyrin macrocycle, where the photocurrent is produced, should have strong electronic coupling to TiO_2. If an anchoring group is linked directly to the macrocycle, the distance is short, and the coupling is strong, and high efficiency is expected. Indeed, this is exactly what happened in Wang's porphyrin DSSCs (η ~5%) (22), where the COOH group was anchored directly to the β position of the macrocycle. In contrast, the COOH groups of the present samples are remotely decoupled from the macrocycle through the phenyl group, resulting in poor electronic coupling. The orientation of the anchoring group with respect to the macrocycle also affects electronic coupling. The preferred orientation is to have the anchoring group parallel to the macrocycle. However, the carboxyphenyl group of the present samples is oriented perpendicular to the porphyrin macrocycle, resulting in poor electronic coupling. Hence, although the absorption bands of the substituted porphyrin have been successfully red-shifted to the infrared region, to improve the conversion efficiency, we need to reduce aggregation of the porphyrin molecules and design anchoring groups with better structure in the future.

4 Conclusions

In conclusion, we have synthesized three new porphyrin derivatives with different numbers of substitution. The optical absorption spectra reveal very large redshift effects and broadening of the absorption energies in response to the substitution. The enhancement of the optical absorption is most pronounced in the long-wavelength visible region. The low energy conversion efficiency is attributed to the aggregation of the porphyrin molecules and the geometry of the anchoring group.

Acknowledgments

The authors would like to thank the National Research Council of the Republic of China, Taiwan, for financially supporting this research under Grant No. NSC97-ET-7-005-002-ET.

References

1. O'Regan, B. and Grätzel, M. (1991) *Nature*, 353, 737–740.
2. Grätzel, M. (2000) *Photovoltaics Prog*., 8, 171–185.
3. Nakade, S., Saito, Y., Kubo, W., Kitamura, T., Wada, Y. and Yanagida, S. (2003) *J. Phys. Chem. B*, 107, 8607–8611.
4. Hara, K., Sato, T., Katoh, R., Furube, A., Ohga, Y., Shinpo, A., Suga, S., Sayama, K., Sugihara, H. and Arakawa, H. (2003**)** *J. Phys. Chem. B*, 107, 597–606.
5. Benkstein, K.D., Kopidakis, N., Van de Lagemaat, J. and Frank, A.J. (2003) *J. Phys. Chem. B,* 107, 7759–7767.
6. Kalyanasundaram, K., Vlachopoulos, N., Krishnan, V., Monnier, A. and Grätzel, M. (1987) *J. Phys. Chem*., 91, 2342–2347.
7. Nazeeruddin, M.K., Kay, A., Rodicio, I., Humphry-Baker, R., Muller, E., Liska, P., Vlachopoulos, N. and Grätzel, M. (1993) *J. Am. Chem. Soc*., 115, 6382–6390.
8. Grätzel, M. (2004) *J. Photochem. Photobiol.* A, 164, 3–14.
9. An excellent description of the natural photosynthetic process is in: R. E. Blankenship, Molecular Mechanisms of Photosynthesis (Blackwell Science Ltd, Oxford, UK, 2002).
10. Liu, Z.M., Yasseri, A.A., Lindsey, J.S. and Bocian, D.F. (2003) *Science*, 302, 1543–1545.
11. Imahori, H., Mori, Y. and Matano, Y. (2003) *J. Photochem. Photobiol. C*, 4, 51–83.
12. Choi, M.S., Yamazaki, T., Yamazaki, I. and Aida, T. (2004) *Chem. Angew., Int. Ed.*, 43, 150–158.
13. Dabestani, R., Bard, A.J., Campion, A., Fox, M.A., Mallouk, T.E., Webber, S.E. and White, J.M. (1988) *J. Phys. Chem*., 92, 1872–1878.
14. Vlachopoulos, N., Liska, P., Mcevoy, A.J. and Grätzel, M. (1987) *Surf. Sci*., 189, 823–831.
15. Odobel, F., Blart, E., Lagree, M., Villieras, M., Boujtita, H., El Murr, N., Caramori, S. and Bignozzi, C.A. (2003) *J. Mater. Chem*., 13, 502–510.
16. Jasieniak, J., Johnston, M. and Waclawik, E.R. (2004) *J. Phys. Chem. B*, 108, 12962–12971.
17. Ma, T.L., Inoue, K., Yao, K., Noma, H., Shuji, T., Abe, E., Yu, J.H., Wang, X.S. and Zhang, B.W. (2002) *J. Electroanal. Chem*., 537, 31–38.
18. Ma, T.L., Inoue, K., Noma, H., Yao, K. and Abe, E. (2002) *J. Photochem. Photobiol. , A,* 152, 207–212.
19. Campbell, W.M., Burrell, A.K., Officer, D.L. and Jolley, K.W. (2004) *Coord. Chem. Rev.*, 248, 1363–1379.

20. Cherian, S. and Wamser, C.C. (2000) *J. Phys. Chem. B*, 104, 3624–3629.
21. Nazeeruddin, M.K., Humphry-Baker, R.K., Officer, D.L., Campbell, W.M., Burrell, A.K. and Grätzel, M. (2004) *Langmuir*, 20, 6514–6517.
22. Wang, Q., Campbell, W.M., Bonfantani, E.E., Jolley, K.W., Officer, D.L., Walsh, P.J., Gordon, K., Humphry-Baker, R.K., Nazeeruddin, M.K. and Grätzel, M. (2005) *J. Phys. Chem. B*, 109, 15397–15409.
23. Campbell, W.M., Jolley, K.W., Wagner, P., Wagner, K., Walsh, P.J., Gordon, K.C., Schmidt-Mende, L., Nazeeruddin, M.K., Wang, Q., Grätzel, M. and Officer, D.L. (2007) *J. Phys. Chem. C*, 111, 11760.
24. Eu, S., Hayashi, S., Umeyama, T., Matao, Y., Araki, Y. and Imahori, H. (2008) *J. Phys. Chem. C*, 112, 4396.
25. Park, J.K., Lee, H.R., Chen, J., Shinokubo, H., Osuka, A. and Kim, D. (2008) *J. Phys. Chem. C*, 112, 16691.
26. Tsuda, A. and Osuka, A. (2001) *Science*, 293, 79.
27. Norsten, T.B., Chichak, K. and Branda, N.R. (2002) *Tetrahedron*, 58, 639–651.
28. Shanmugathasan, S., Johnson, C.K., Edwards, C. Matthews, E.K., Dolphin, D. and Boyle, R.W. (2000) *J. Porphyr. Phthalocya*., 4, 228–232.
29. Kelkar, A.A., Patil, N.M. and Chaudhari, R.V. (2002) *Tetrahedron Lett*., 43, 7143–7146.
30. Lambert, C. and Nöll, G. (2002) *J. Chem. Soc., Perkin Trans*., 2, 2039–2043.
31. Gryko, D.T., Clausen, C., Roth, K.M., Dontha, N., Bocian, D.F., Kuhr, W.G. and Lindsey, J.S. (2000) *J. Org. Chem*., 65, 7345–7355.
32. Lambert, C., Nöll, G., Schmälzlin, E., Meerholz, K. and Bräuchle, C. (1998) *Chem. Eur. J*., 4, 2129–2135.
33. Cramariuc, O., Hukka, T.I. and Rantala, T. (2004) *Chem. Phys*., 305, 13–26.
34. Kittel, C. Introduction to Solid State Physics, 7th Ed., John Wiley & Sons: New York, 1996, p. 330.
35. Vittadini, A., Selloni, A., Rotzinger, F.P. and Grätzel, M. (2000) *J. Phys. Chem. B*, 104, 1300–1306.
36. Tachibana, T., Haque, S.A., Mercer, I.P., Durrant, J.R. and Klug, D.R. (2000) *J. Phys. Chem. B*, 104, 1198–1205.
37. Tatay, S., Haque, S.A., O'Regan, B., Durrant, J.R., Verhees, W.J.H., Kroon, J.M., Vidal-Ferran, A., Gaviña, P. and Palomares, E. (2007) *J. Mater. Chem.,* 17, 3037–3044.
38. Wang, Z.S., Cui, Y., Dan-oh, Y., Kasada, C., Shinpo, A. and Hara, K. (2007) *J. Phys. Chem. C*, 111, 7224–7230.